An Asymptotic Approach for the Scan Impedance in Infinite Phased Arrays of Dipoles

A.J. Pascual, R. Sauleau, D. Gonzalez-Ovejero

An Asymptotic Approach for the Scan Impedance in Infinite Phased Arrays of Dipoles

Álvaro J. Pascual, Ronan Sauleau, *Fellow, IEEE,* and David González-Ovejero, *Senior Member, IEEE*

***Abstract*—This work presents an analytic model to derive the scan impedance of planar infinite phased arrays of dipoles at a dielectric interface when only the $(0,0)$ Floquet mode propagates. The proposed model builds on the boundary conditions met by the fundamental Floquet mode at the interface to provide a novel derivation of the equivalent circuit for the scan impedance. The analysis is also extended to include the effect of a sufficiently thick grounded substrate that does not affect the elements current distribution and does not interact with the evanescent fields. Next, formulas for the ratio of intensity radiated towards each half-space for an interfacial array are provided. In a consecutive step, an asymptotic approximation is derived for the current distribution in arrays of arbitrary loaded dipoles, and the reactance of a dipole in the array environment is related to the inductance of a grid of wires. This model constitutes a useful tool to clearly identify the role of the different array variables (dipole dimensions, relative permittivity of the substrate, periodicity, end-load, and scan angle in the principal planes) on the scan impedance by simple expressions and equivalent circuits. The model predictions are in good agreement with full-wave simulations and with previously published works.**

***Index Terms*—Equivalent circuit, scan impedance, infinite array, phased array, dipole array, planarly layered media, plane wave expansion.**

I. Introduction

PHASED arrays represent a broad class of antennas to which extensive research efforts have been dedicated [1]–[3]. In particular, planar phased arrays of printed elements, such as dipoles or slots, have received most of the attention. Wide-band, dual-linear, and wide-scan performance have been reported for connected or tightly coupled arrays of dipoles [4]–[6].

As the number of elements in the array increases for a fixed element spacing, the central elements behave like those within an infinite array [7], [1, Ch. 7]. Thus, the infinite array approach is an analysis method suitable for large arrays where edge elements and edge-related effects do not substantially affect the overall performance.

The authors are with Univ Rennes, CNRS, IETR (Institut d'Électronique et des Technologies du numéRique)- UMR 6164, F-35000, Rennes, France. E-mail: alvaro-jose.pascual, ronan.sauleau, david.gonzalez-ovejero@univ-rennes1.fr.

Manuscript received Month DD, 2020; revised Month DD, YYYY; accepted Month DD, YYYY. Date of publication Month DD, YYYY. (Correspnding author: D. González-Ovejero).

This work is supported by the European Union through the European Regional Development Fund (ERDF), and by the French region of Brittany, Ministry of Higher Education and Research, Rennes Métropole and Conseil Départemental 35, through the CPER Project SOPHIE / STIC & Ondes.

Digital Object Identifier XXXXXXXXXXXXXXXXXX.

Previous studies on infinite phased arrays of dipoles are numerous. Indeed, the periodicity of the array enables the expansion of the fields in a discrete set of plane waves or Floquet modes (spectral approach). This approach generally leads to simplified mathematical expressions that can be readily evaluated numerically or even analytically in some cases. In [8], the current sheet model was presented as the simplest infinite phased array in the limiting case of closely spaced Hertzian dipoles. This model led to simple expressions for the scan resistance, and the concept was later extended in [9] for printed elements on a semi-infinite dielectric interface. Arrays of disconnected dipoles in free-space were considered either assuming a current distribution [10], [11], [12, Ch. 3], or by an integral equation technique [13]. Later on, the study was extended to solve disconnected dipoles printed on semi-infinite substrates or on a grounded dielectric slab using a Method of Moments (MoM) [14]. Since then, extensive numerical studies, implementations, and theoretical modeling of connected or tightly coupled arrays have been carried out, for instance in [15]–[21]. Of special relevance are the works by Munk and collaborators [22], [23] based on a periodic MoM approach to determine expressions for the dipole scan impedance. However, in the aforementioned studies, the arrays in multilayered media were always embedded in a homogeneous region, and never at the interfaces, as it is usually the case in practical realizations.

Despite the extensive efforts devoted in the past to the analysis of infinite phased arrays of dipoles, to date, there is no model to readily interpret the impact of the array variables on the scan impedance, especially on the reactance. The numerical methods such as those in [14], [22], [24] or the description in [19], are rigorous and computationally powerful but mask the fundamental impedance features of the array. Therefore, one is forced to carry out exhaustive computation and parametric sweeps to gain physical insight into the array operation for different configurations. For instance, the spectral expansion approach by [22] yields a double infinite sum to calculate the scan reactance. From this, general conclusions can be hardly inferred. On the other hand, an approximate analytic method is more appropriate to evaluate in a simple manner how the different phenomena affect the scan impedance for diverse array configurations. We provide in this paper a novel and insightful circuit approach that readily shows the role of the main variables of a phased array of dipoles on the scan impedance as defined in [1, Ch. 1]. These variables include the dipole dimensions and type of end-load,

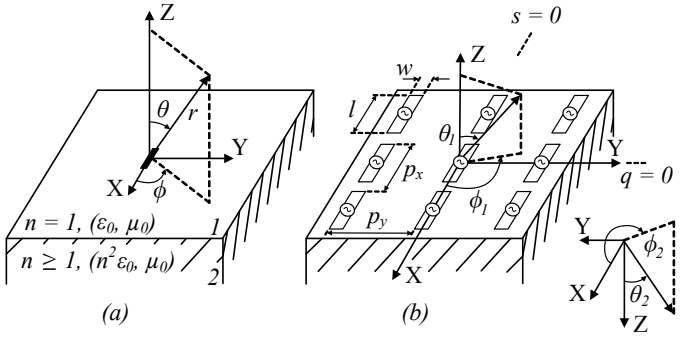

Fig. 1. (a) Hertzian dipole printed on the interface between two lossless dielectrics. Medium 1 ($z > 0$) is characterized by $n = 1$ and medium 2 ($z < 0$) is characterized by $n \geq 1$. (b) Cut of the infinite interfacial array of dipoles in a rectangular lattice, relevant geometrical parameters, and the respective coordinate system for each half-space.

the array periodicity, the relative permittivity of the substrate for a printed array, and the scan angle in the principal planes. Although the Green's function approach was used in [18] to derive equivalent circuits for interfacial arrays of connected dipoles, the circuits and expressions in this work stem instead from the boundary conditions met by the fundamental Floquet mode and an asymptotic approximation of the current, which can handle arbitrary loads.

The paper is organized as follows: In Section II, we exploit the far-field plane wave expansion of a dipole array on an interface to obtain boundary conditions at the interface for the radiated fundamental Floquet mode. In Section III, the boundary conditions are used to obtain equivalent networks and expressions for the scan resistance when the array lies at a dielectric interface. The ratio of intensity radiated towards each half-space is also derived. In Section IV, the analysis is extended to cases where a ground plane backs the interfacial array. We assume a thick substrate so that the ground plane does not affect the elements current distribution and it does not interact with the evanescent fields. Such assumptions are fulfilled by a typical substrate thickness of $\lambda/4$. Next, Section V is devoted to the derivation of the current along the dipole and an equivalent network for the scan reactance at broadside. The results obtained with the proposed model are compared to full-wave simulations in Section VI, followed by the results for the principal scan planes in Section VII. We conclude the analysis with remarks on the scan impedance and general conclusions in Sections VIII and IX, respectively.

II. Plane Wave Expansion on the Radiated Fields

In order to derive the electric field radiated by an infinite phased array of dipoles lying on a dielectric interface, first we add the individual contributions of interfacial Hertzian dipoles. Then, this sum is written in the spectral domain as a discrete set of plane waves or Floquet modes. We will show that the tangential electric field is equal at both sides of the interface for the fundamental Floquet mode. This result will constitute the basis of the subsequent discussion.

The electric field of a Hertzian dipole in a homogeneous medium admits a closed-form expression both in the near- and far-field regions. This is not the case for a dipole placed parallel, and at the interface between two different dielectrics. This hurdle, however, can be conveniently overcome using the far-field of the interfacial Hertzian dipole in [25]. The Hertzian dipole is of length Δl, its current I, and the interface is composed of two lossless dielectrics as shown in Fig. 1(a). The upper dielectric is characterized by $n_1 = 1$ and the lower one by $n_2 = n \geq 1$. That is, the ratio of dielectric index is n. For a harmonic time dependence $\mathrm{e}^{\mathrm{j}\omega t}$, the expression is written as

$$dE_i^{\theta,\phi} = \frac{\mathrm{j}k_0 n_i I \Delta l}{2\pi} Z_0 f_i^{\theta,\phi}(\theta,\phi) \frac{\mathrm{e}^{-\mathrm{j}n_i k_0 r}}{r}, \tag{1}$$

where i denotes the medium, and Z_0 is the impedance of a TEM wave in free-space. Expression (1) is valid when $k_0 r \to \infty$ and $0 \leq \theta \leq \pi/2$ in medium 1, and when $nk_0 rs \to \infty$ and $\pi - \theta_c \leq \theta \leq \pi$ in medium 2. The angle θ_c is obtained from $\sin\theta_c = 1/n$, and it will be the maximum scan angle allowed in medium 2. The pattern functions in (1) are defined as

$$f_1^{\theta} = \left\{ \frac{\cos^2\theta}{\cos\theta + (n^2 - \sin^2\theta)^{1/2}} - \sin^2\theta\cos\theta \cdot \frac{\cos\theta - (n^2 - \sin^2\theta)^{1/2}}{n^2\cos\theta + (n^2 - \sin^2\theta)^{1/2}} \right\} \cos\phi \tag{2a}$$

$$f_1^{\phi} = -\frac{\cos\theta\sin\phi}{\cos\theta + (n^2 - \sin^2\theta)^{1/2}} \tag{2b}$$

$$f_2^{\theta} = \left\{ \sin^2\theta\cos\theta \frac{(1 - n^2\sin^2\theta)^{1/2} + n\cos\theta}{n(1 - n^2\sin^2\theta)^{1/2} - \cos\theta} - \frac{\cos^2\theta}{(1 - n^2\sin^2\theta)^{1/2} - n\cos\theta} \right\} \cos\phi \tag{2c}$$

$$f_2^{\phi} = \frac{\cos\theta\sin\phi}{(1 - n^2\sin^2\theta)^{1/2} - n\cos\theta}, \tag{2d}$$

where the subscript and superscript in f refer to the corresponding medium and polarization, respectively.

The Hertzian element is now replicated to form a double infinite array of dipoles in a rectangular lattice. The element periodicity is given by p_x and p_y, as shown in Fig. 1(b). The dipoles of length l and width w are centered-fed by ideal δ-gap generators with uniform current amplitude and linear phase progression, defined for the (q,s) element as $I_{qs} = I_{00}\mathrm{e}^{-\mathrm{j}q\Delta\alpha}\mathrm{e}^{-\mathrm{j}s\Delta\beta}$. I_{00} is the current of the $(0,0)$ element, located at the origin of coordinates, and the phase progression is defined (recall $n_1 = 1$):

$$\Delta\alpha = p_x k_1 \sin\theta\cos\phi = p_x k_0 s_x, \tag{3a}$$

$$\Delta\beta = p_y k_1 \sin\theta\sin\phi = p_y k_0 s_y. \tag{3b}$$

The electric far-field of the array is obtained by summation of all individual contributions of the Hertzian elements and double application of Poisson's sum formula. Following a procedure similar to [22, Ch. 4], we have

$$E_i = \frac{Z_0}{p_x p_y} \sum_{u=-\infty}^{+\infty} \sum_{v=-\infty}^{+\infty} \frac{f_i(\theta,\phi)}{s_z} \mathrm{e}^{\pm\mathrm{j}k_i z s_z} \mathrm{e}^{-\mathrm{j}k_0 x\left(s_x + u\left(\frac{\lambda_0}{p_x}\right)\right)} \mathrm{e}^{-\mathrm{j}k_0 y\left(s_y + v\left(\frac{\lambda_0}{p_y}\right)\right)} \int_{-l/2}^{l/2} I(x') \mathrm{e}^{\mathrm{j}k_0 x'\left(s_x + u\left(\frac{\lambda_0}{p_x}\right)\right)} dx', \tag{4}$$

with

$$s_z = \sqrt{1 - \left(\frac{s_x}{n_i} + u\left(\frac{\lambda_i}{p_x}\right)\right)^2 - \left(\frac{s_y}{n_i} + v\left(\frac{\lambda_i}{p_y}\right)\right)^2}. \quad (5)$$

In (4), $z \lessgtr 0$, and the sign in the exponential is taken accordingly for propagation away from the interface. The polarization superscripts in E and in the pattern functions have been omitted, and we have assumed that the current flows along the longitudinal axis of the dipole.

Equation (4) is the electric field resultant from the addition of the far-fields of Hertzian dipoles. It yields a discrete sum of plane waves or Floquet modes with wavevector components at a discrete set of directions in space. For s_z real, the (u, v) mode propagates and decays exponentially otherwise. Note the total electric field is weighed by the dipole pattern function, according to the principle of pattern multiplication.

If the scan angle in medium 2 is limited below θ_c, the $(0, 0)$ Floquet mode always propagates in both media. In addition, if the spacing is such that the other modes do not propagate, the $(0, 0)$ mode in (4) corresponds to the electric field of the radiated plane wave, and is the only term contributing to the scan resistance. The remainder of terms represent the contribution of the Hertzian dipole far-field to the scan reactance in the array environment.

Let us now focus on the propagating term. One can note that the excitation, as defined in (3), determines the wavevector components, s_x, s_y of the $(0, 0)$ Floquet mode. To obtain a simpler expression for the radiated field, it is convenient to use a different reference system for each half-space, as shown in Fig. 1(b). To that end, we apply the the following transformations: $\theta_1 = \theta$, $\phi_1 = \phi$ in medium 1, and $\theta_2 = \pi - \theta$, $\phi_2 = -\phi$ in medium 2. The angles of propagation of the $(0, 0)$ mode in each medium are related by $\phi_2 = -\phi_1$ and $n \sin\theta_2 = \sin\theta_1$. In view of the previous discussion, the radiated electric field in each half-space is expressed as

$$E_i = \frac{Z_0}{p_x p_y} f_i(\theta_i, \phi_i) \frac{\mathrm{e}^{-\mathrm{j}\vec{k_i}\vec{r_i}}}{\cos\theta_i} \int_{-l/2}^{l/2} I(x') \mathrm{e}^{\mathrm{j}k_0 x' s_x} dx', \quad (6)$$

where $\vec{r_i}$ is the observation point in each coordinate system, $\vec{k_1} = k_0(s_x, s_y, \cos\theta_1)$, and $\vec{k_2} = k_0(s_x, -s_y, n\cos\theta_2)$. At broadside, it is not difficult to see that $E_1 = E_2$ at the interface plane ($z_i \to 0^+$). Similarly, comparing in (6) for both media, after some algebra, one finds the following relations

$$E_{1\theta} \cos\theta_1 = E_{2\theta} \cos\theta_2, \qquad E_{1\phi} = -E_{2\phi}. \quad (7)$$

The relations are valid for any scan angle (recall $0 \le \theta_2 < \theta_c$, or equivalently, $0 \le \theta_1 < \pi/2$). Therefore, the tangential component of the electric field is equal at both sides of the interface for the fundamental Floquet mode, analogously to the classical boundary condition. We will also refer to (7) as boundary condition even if this expression is true in the far-field. In general, (7) is valid for any two loss-less dielectrics characterized by n_1 and $n_2 \ge n_1$, with θ_1 and θ_2 related by the Snell's law. The minus sign for $E_{2\phi}$ in (7) appears given that $\hat{\phi}_i$ are reversed as measured from system of reference 2 with respect to system of reference 1.

The boundary conditions in (7) have been derived for the mode that concerns our present study. However, it is not difficult to demonstrate that the continuity of the tangential component of the electric field across the interface is fulfilled by all modes individually, except for a $-\mathrm{j}$ factor if the mode decays in medium 1 but not in 2. This stems from the fact that the plane wave decomposition results in the fields being expressed as a sum of propagating or evanescent plane waves fulfilling the classical boundary conditions.

Equation (7) will be used in the next section to derive expressions and equivalent networks for the scan resistance of dipoles in an infinite phased array, and also to calculate the intensity radiated towards each half-space.

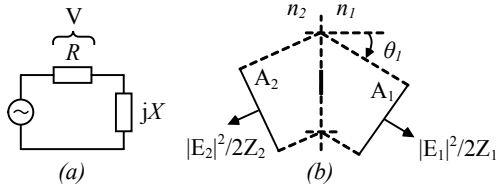

Fig. 2. The power dissipated in the scan resistance of the dipole (a), corresponds to the power carried away by the radiated mode in the apparent area allocated for the element (b).

III. Array on a Dielectric Interface

In this section, the structure depicted in Fig. 1(b) is studied. The generators excite the array impressing a fixed voltage, or current, at the dipole input terminals. Ohmic losses are neglected, and the dielectric half-spaces are generally characterized by n_1 and $n_2 \ge n_1$. The corresponding impedances for a TEM wave are Z_1 and Z_2. The periodicity is such that grating lobes are precluded, and the allocated area for each element is $p_x p_y$.

A. Scan Resistance at Broadside

The scan resistance at broadside can be derived through (7). For the radiated plane wave, we have $E_{1\theta} = E_{2\theta} = E$. Let V be the voltage drop in the scan resistance of a reference dipole, R_r, as in the equivalent circuit of Fig. 2(a). The power dissipated in the resistance equals the total Poynting vector times the element allocated area (Fig. 2(b) for $\theta_1 = 0$). Omitting the factor 1/2 from time average, we have

$$\frac{|V|^2}{R_r} \frac{1}{p_x p_y} = \frac{|E|^2}{Z_1} + \frac{|E|^2}{Z_2}. \quad (8)$$

For an emitted plane wave, the electric field is related to the voltage at the dipole terminals by $V = P_f E$ [22, eq. 4.45], where E is the electric field parallel to the dipole ($\hat{x}$-directed). Since the tangential component is continuous across the interface, there is no ambiguity in the choice of E. P_f is defined as

$$P_f = \frac{1}{I(0)} \int_{-l/2}^{l/2} I(x') \mathrm{e}^{\mathrm{j}k_1 x' s_x} dx'. \quad (9)$$

Bear in mind that k_1 appears in the expression above because medium 1 is chosen to define the phase progression (in turn defining s_x). The integral is performed over any element of the array, with $I(0)$ the current at the feed point. Relating E and V in (8) gives

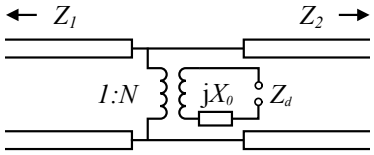

Fig. 3. Equivalent network for the scan impedance of an infinite interfacial phased array of dipoles.

$$R_r = (Z_1 \parallel Z_2)\frac{|P_f|^2}{p_x p_y}. \tag{10}$$

B. Scan Resistance for Principal Scan Planes

Let us now examine how the scan resistance varies at the principal scan planes. As explained above, the power delivered to R_r equals the total Poynting vector times the apparent or projected area allocated for the element. Thus we have

$$R_r = \frac{|P_f|^2}{p_x p_y}\frac{Z_0}{\dfrac{n_1}{\cos\theta_1}+\dfrac{n_2}{\cos\theta_2}} = N^2(Z_1\cos\theta_1 \parallel Z_2\cos\theta_2), \tag{11a}$$

$$R_r = \frac{|P_f|^2}{p_x p_y}\frac{Z_0}{n_1\cos\theta_1+n_2\cos\theta_2} = N^2\left(\frac{Z_1}{\cos\theta_1} \parallel \frac{Z_2}{\cos\theta_2}\right), \tag{11b}$$

where (11a) and (11b) stand for E- and H-plane scan respectively. Arbitrary scan angles shall be treated similarly, and noting that $E_{1\theta}/E_{1\phi} = f_{1\theta}/f_{1\phi}$, which is known analytically. The shunt impedance in (10) indicates that the scan resistance can be expressed in terms of an equivalent network composed of two shunt infinite transmission lines (TLs), while the factor $|P_f|^2/p_x p_y = N^2$ is accounted for by a transformer. At broadside, the scan impedance, Z_d, corresponds to the equivalent network of Fig. 3, and by transforming $Z_i \to Z_i\cos\theta_i$, $Z_i \to Z_i/\cos\theta_i$, analog networks follow for E- and H-plane scan respectively. X_0 in the equivalent network accounts for the scan reactance, and depends in general on n_1 and n_2, the array geometry, the scan angle, and the frequency. Note that the current distribution is also required to calculate P_f and in turn the scan resistance. These two aspects will be studied in Section V. For a homogeneous medium, we obtain a result equivalent to those obtained in [12], [22].

C. The Intensity Radiated Toward Each Half-Space

Let us now examine the ratio of intensity (S) radiated toward each half space. For H-plane scan, using (7) one can easily obtain $S_1 = n_1|E_{1\phi}|^2/Z_0$, and $S_2 = n_2|E_{1\phi}|^2/Z_0$. Hence:

$$\frac{S_2}{S_1} = \frac{n_2}{n_1}. \tag{12}$$

In this plane, the ratio is constant with the scan angle. For an air-dielectric interface, it equals $\epsilon_r^{1/2}$, with ϵ_r the relative permittivity of the dielectric. For E-plane scan, $S_1 = n_1|E_{1\theta}|^2/Z_0$, and $S_2 = n_2|E_{2\theta}|^2/Z_0$. Then, using (7):

$$\frac{S_2}{S_1} = \frac{n_2\cos^2\theta_1}{n_1\cos^2\theta_2}. \tag{13}$$

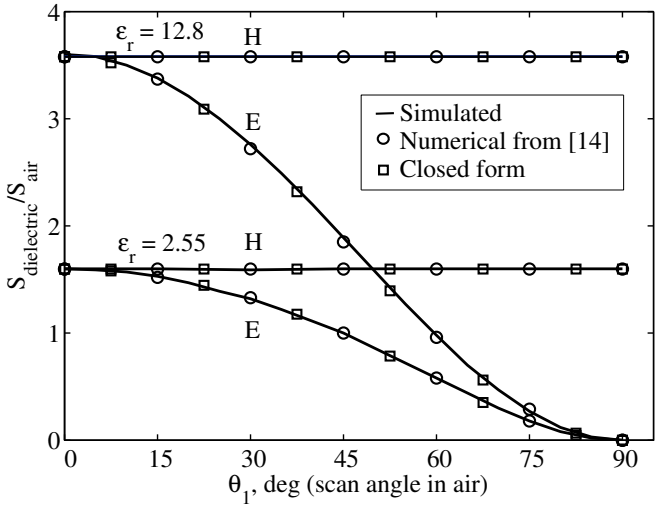

Fig. 4. Ratio of Poynting vector modulus in the principal planes for the mode radiated by an infinite phased array of dipoles. We consider two different air-dielectric interfaces: Duroid ($\epsilon_r = 2.55$) and GaAs ($\epsilon_r = 12.8$). Full-wave simulations with ANSYS HFSS [26] (solid lines), present model (squares), and numerical calculation from [14] (circles). The dimensions are $p_x = p_y = 0.2184\lambda_0$, $l = 0.182\lambda_0$, $w = 0.01\lambda_0$.

The ratio of intensity is in general different from that of a single dipole, which equals $\epsilon_r^{3/2}$ at broadside for an air-dielectric interface, as can be inferred from (1)-(2), and also noted in [14]. Fig. 4 shows the intensity ratio calculated by (12)-(13) for two different air-dielectric interfaces. Results practically overlap with full-wave simulations and are in good agreement with those calculated in [14, Fig. 9]. The power ratio would be obtained by multiplying S times the projected area allocated for each element in the direction of the scan angle. In particular, at broadside both projected areas coincide and the power ratio also equals $\epsilon_r^{1/2}$ for an air-dielectric interface. Since at broadside $E_1 = E_2$, the ratio must be the same for any planar antenna regardless of its current distribution, even if the antenna is not linear.

IV. Array on a Dielectric Interface Backed by a Ground Plane

Since the initial radiated fields are known by the boundary conditions, it is possible to account for the effect of a ground plane reflector by computing the multiple reflections. Calculation of the real and complex power leads to expressions for the scan impedance for broadside and for the principal scan planes. It is assumed that the reflector is placed at a distance d from the interface in any medium, say medium 2, such that the evanescent modes do not interact with it and that its presence does not alter the current distribution of the elements. For the sake of simplicity, the broadside case is treated first and the expressions for E- and H-plane scan are derived next by analogy. Under the previous assumptions, the scan impedance is written as the sum of three terms: X_0, the initial reactive part, R_r^{GP} , a term related to the amplitude of the plane wave emerging from the structure and, X^{GP}, related to the reactive energy stored due to the presence of the ground plane:

$$Z_d = R_r^{\mathrm{GP}} + \mathrm{j}X^{\mathrm{GP}} + \mathrm{j}X_0. \tag{14}$$

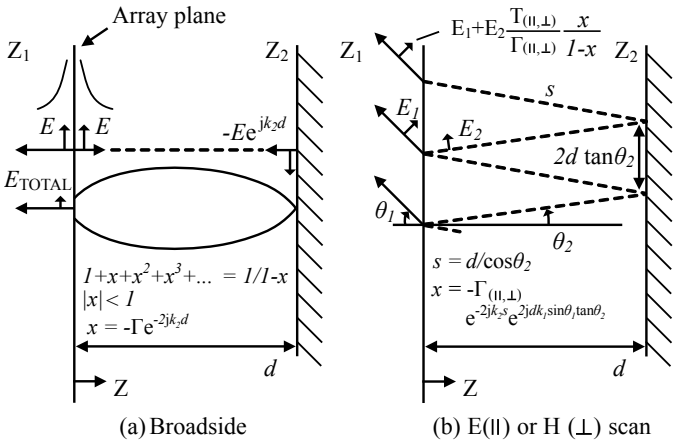

(a) Broadside (b) E(||) or H (⊥) scan

Fig. 5. Longitudinal cut of the infinite dipole array backed by a groundplane at a distance d. (a) Broadside emission (top-bottom): evanescent fields in z-direction do not interact with the groundplane, initially radiated fields, resultant electric field from the partially standing wave, and sum formula for multiple reflections. (b) E- or H-scan (top-bottom): emerging field at the interface plane after multiple reflections, initially radiated fields, and directions of propagation.

A. Scan Impedance at Broadside

The situation where the array radiates at broadside is depicted in Fig. 5(a).

1) Real Power and Resistance: The resultant electric field emerging from the structure at the interface plane, after consideration of the multiple reflections, is given by

$$E_{\text{total}} = E\left(\frac{1-\mathrm{e}^{-2\mathrm{j}k_2 d}}{1+\Gamma\mathrm{e}^{-2\mathrm{j}k_2 d}}\right), \tag{15}$$

where Γ is the Fresnel's reflection coefficient from medium 2 to 1 for normal incidence:

$$\Gamma = \frac{n_2 - n_1}{n_2 + n_1}. \tag{16}$$

The power radiated per allocated element area is

$$\frac{|I(0)|^2}{p_x p_y} R_r^{\text{GP}} = \frac{|E|^2}{Z_1}\left|\frac{1-\mathrm{e}^{-2\mathrm{j}k_2 d}}{1+\Gamma\mathrm{e}^{-2\mathrm{j}k_2 d}}\right|^2. \tag{17}$$

On the other hand, the power delivered to each element per allocated area when there is no ground plane is given by

$$\frac{|I(0)|^2}{p_x p_y} R_r = \frac{|E|^2}{Z_1 \parallel Z_2}, \tag{18}$$

combining (17) and (18), one obtains

$$R_r^{\text{GP}} = R_r \frac{n_2/n_1 + 1}{1 + \left(\dfrac{n_2}{n_1 \tan(k_2 d)}\right)^2}. \tag{19}$$

For a homogeneous medium, (19) reduces to $R_r^{\text{GP}} = 2R_r \sin^2(k_2 d)$. Examination of (19) indicates that for $k_2 d = m\pi$, with $m = 0, 1, 2...$, the ground plane short-circuits the array and the scan resistance equals 0. The positions of maximum scan resistance occur at $k_2 d = (2m+1)\pi/2$ and yield $R_r^{\text{GP}} = R_r(1 + n_2/n_1)$. Finally, for $\tan^2(k_2 d) = n_2/n_1$, the ground plane leaves the scan resistance of the array untouched, $R_r^{\text{GP}} = R_r$. The first position occurs at $d = \lambda/8$ for a homogeneous medium (radiated field to the left and reflected add in quadrature), but the position deviates when the array is at an interface.

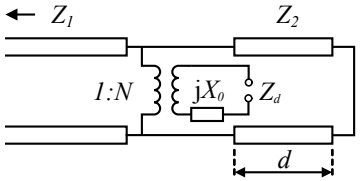

Fig. 6. Equivalent network for the scan impedance of an infinite interfacial phased array of dipoles backed by a ground plane.

2) Complex Power and Reactance: To calculate the reactive part associated with the presence of the ground plane, first, the resulting fields inside the structure are computed:

$$E_{\text{total}} = \frac{E}{1+\Gamma\mathrm{e}^{-2\mathrm{j}k_2 d}}\left(\mathrm{e}^{-\mathrm{j}k_2 z} - \mathrm{e}^{-\mathrm{j}k_2 d}\mathrm{e}^{\mathrm{j}k_2(z-d)}\right), \tag{20a}$$

$$H_{\text{total}} = \frac{E}{Z_2(1+\Gamma\mathrm{e}^{-2\mathrm{j}k_2 d})}\left(\mathrm{e}^{-\mathrm{j}k_2 z} + \mathrm{e}^{-\mathrm{j}k_2 d}\mathrm{e}^{\mathrm{j}k_2(z-d)}\right), \tag{20b}$$

where $0 \le z \le d$. The calculation of the reactive power, P_X, per allocated area yields

$$\begin{aligned}\frac{P_X}{p_x p_y} &= \frac{\partial\left(\int_0^d (W_e - W_m)dx\right)}{\partial t} \\ &= \mathrm{j}\frac{|E|^2}{Z_2|1+\Gamma\mathrm{e}^{-2\mathrm{j}k_2 d}|^2}\sin(2k_2 d).\end{aligned} \tag{21}$$

W_e and W_m are, respectively, the electric and magnetic energy densities. Comparing the reactive power delivered to the reactance X^{GP} by the ideal current generator and the power delivered to the scan resistance when there is no reflector (18), yields

$$X^{\text{GP}} = R_r \frac{n_1 + n_2}{2\left(n_2\cos^2(k_2 d) + \dfrac{n_1^2}{n_2}\sin^2(k_2 d)\right)}\sin(2k_2 d). \tag{22}$$

When the initially radiated field adds in phase with the reflections, the scan resistance is maximum and X^{GP} equals 0. X^{GP} takes this value again when the ground plane short-circuits the antenna; then the zeros of X^{GP} occur for $k_2 d = m\pi/2$. X^{GP} takes extreme values larger than $\pm R_r$ when $Z_2 < Z_1$ and lower otherwise. For a homogeneous medium, (22) reduces to $X^{\text{GP}} = R_r \sin(2k_2 d)$, and X^{GP} takes values between $\pm R_r$. In particular, when R_r^{GP} equals R_r, so does $|X^{\text{GP}}|$.

Finally, it can be seen that (14), where R_r^{GP} is given by (19), and X^{GP} is given by (22), corresponds to the input impedance of the equivalent network of Fig. 6.

B. Scan Impedance for Principal Scan Planes

Let the array now scan in a principal plane that corresponds to an angle θ_1 in medium 1.

1) Real Power and Resistance: The resultant electric field emerging from the structure at the interface plane, after addition of the multiple reflections (see Fig. 5(b)) is

$$E_{\text{total}} = E_1 \left(\frac{1 - \mathrm{e}^{-2\mathrm{j}k_2 d\cos\theta_2}}{1 + \Gamma_{\parallel,\perp}\mathrm{e}^{-2\mathrm{j}k_2 d\cos\theta_2}} \right), \tag{23}$$

where the relation $\Gamma_\perp - T_\perp = \Gamma_\parallel - T_\parallel \cos\theta_1/\cos\theta_2 = -1$ has been used to compute the sum, with T being the electric field transmission coefficient from medium 2 to 1. The subscripts $\perp, \parallel$ denote TE and TM polarization for the H- and E-plane respectively. In turn, the Fresnel reflection coefficients are given by

$$\Gamma_\perp = \frac{n_2\cos\theta_2 - n_1\cos\theta_1}{n_2\cos\theta_2 + n_1\cos\theta_1}, \tag{24a}$$

$$\Gamma_\parallel = \frac{n_2/\cos\theta_2 - n_1/\cos\theta_1}{n_2/\cos\theta_2 + n_1/\cos\theta_1}. \tag{24b}$$

By substituting $d \to d\cos\theta_2$, $Z_i \to Z_i\cos\theta_i$ (E-plane), $Z_i \to Z_i/\cos\theta_i$ (H-plane) in (15) and (16), one retrieves (23) and (24). Then, applying these transformations in (19) suffices to obtain R_r^{GP} in the principal scan planes.

2) Complex Power and Reactance: The electric field within the structure can be written as

$$E_{\text{total}} = \frac{E_2}{1 + \Gamma_{\parallel,\perp}\mathrm{e}^{-2\mathrm{j}k_2 d\cos\theta_2}} \left(\mathrm{e}^{-\mathrm{j}k_2 z\cos\theta_2}\hat{u}_+ - \mathrm{e}^{-\mathrm{j}k_2(z-d)\cos\theta_2}\mathrm{e}^{\mathrm{j}k_2(z-d)\cos\theta_2}\hat{u}_- \right), \tag{25}$$

where $\hat{u}_\pm = \hat{y}\cos\theta_2 \mp \hat{z}\sin\theta_2$, and $\hat{u}_\pm = \hat{x}$ for E- and H-plane scan respectively. In turn, the reactive power per allocated element area is given by

$$\frac{P_X}{p_x p_y} = \mathrm{j}\frac{|E_2|^2\cos\theta_2}{Z_2|1 + \Gamma_{\parallel,\perp}\mathrm{e}^{-2\mathrm{j}k_2 d\cos\theta_2}|^2}\sin(2k_2 d\cos\theta_2). \tag{26}$$

After comparing (26) with (21) and the Fresnel's reflection coefficients, it is found that X^{GP} in the principal scan planes can be also obtained applying in (22) the transformations: $d \to d\cos\theta_2$, $Z_i \to Z_i\cos\theta_i$ (E-plane), $Z_i \to Z_i/\cos\theta_i$ (H-plane). Since both the real and imaginary parts transform the same for either E- or H-plane scan, the equivalent networks and conclusions are analog to those drawn for the broadside case in Section IV-A.

Although we have treated here the case of an array backed by a ground plane reflector, a similar treatment can be developed for other structures (i.e. grids [27] or an arbitrary impedance sheet) where the reflection coefficients are known for TE and TM polarization. In particular, one can observe that the radiated plane wave propagates along the layers of the structure much like a TEM wave does on a TL with different segments and loads. Then, it is possible to extend the equivalent networks presented here to multilayered structures as long as their equivalent network is known in terms of plane wave propagation with the corresponding polarization.

Finally, note that a grounded dielectric slab may introduce additional solutions of propagation in the form of surface waves, potentially causing scan blindness [28]. A condition for this to occur is that the k-vector component of a radiated mode along the interface, k_t, matches the propagation constant of the surface wave, β_{SW}. Nevertheless, the scan angle in the medium 1 (recall $n_1 \leq n_2$) is limited below 90°, so $k_t < k_1$ for the fundamental Floquet mode, with $k_1 \leq \beta_{\text{SW}}$. Hence, it cannot excite a surface wave and it is necessary that at least a grating lobe exists. The assumption that only the $(0,0)$ Floquet mode propagates precludes the appearance of this phenomenon.

V. Asymptotic Current Approximation

The plane wave expansion in (6) has enabled the derivation of expressions and equivalent networks for the scan resistance and the reactance term due to a ground plane, if present. To compute them, however, the dipole current distribution must be known, so that it can be inserted in (9). In addition, only the far-field from the Hertzian dipole has been accounted for in the plane wave expansion. Hence, the decaying terms in the sum of (4) do not represent the total evanescent fields, and the Poynting theorem [10] cannot be used to calculate X_0. This section is devoted to the analysis of the scan reactance and current distribution.

Let us start by examining the current distribution along one row of the array presented in Fig. 1(b). In the most general case, the dipoles can be connected through lumped loads of impedance Z_L. The load can be an open circuit (disconnected arms with moderate gap), a short-circuit (connected arms) or an interdigitated capacitor [29]. For convenience, we assume the q element centered at the origin of coordinates as shown in Fig. 7(a).

In the source-free regions of a linear antenna, it was demonstrated in [30, Ch. 8] that the current satisfies ordinary TL equations when the dipole width $w \to 0$, and the effect of radiation resistance on the current is neglected. Under these assumptions, hereinafter referred to as asymptotic approximation, one can write

$$\frac{\mathrm{d}^2 I_q(x)}{\mathrm{d}x^2} + \beta^2 I_q(x) = 0. \tag{27}$$

$I_q(x)$ denotes the current along the row due to the q generator, with all others disconnected, and β is the propagation constant in the medium in which the array is located [30, Ch. 8]. The interface can be simply treated as an homogeneous medium of effective dielectric constant [14] $\epsilon_{\text{eff}} = (\epsilon_1 + \epsilon_2)/2$. We define the source-free domain as $\Omega := x \in \mathbb{R} - \{ml\}$, $m \in \mathbb{Z}$. That is, the length of the row except the points where the sources are located. The corresponding boundary consists of the positions of the generators $(x = ml)$.

To solve for the total current along the row, $I(x)$, it suffices to solve (27) and later apply superposition with the proper phased excitation, as shown schematically in Fig. 7(b). Equation (27) is a homogeneous Helmholtz equation which general solution is well known. To solve it we apply Dirichlet boundary conditions such that $\forall x \in \partial\Omega - \{0\}$, $I_q(x) = 0$ and $I_q(0) = I(0)\mathrm{e}^{-\mathrm{j}q\Delta\alpha}$. We also enforce the continuity of the current. It is not difficult to see that $I_q(x) = 0$ for $|x| \geq l$. In addition, by symmetry, $I_q(x) = I_q(-x)$, so actually we only need to solve for $0 \leq x \leq l$, as in Fig. 7(c). This region corresponds to the right arm of dipole q and left arm of dipole $q+1$.

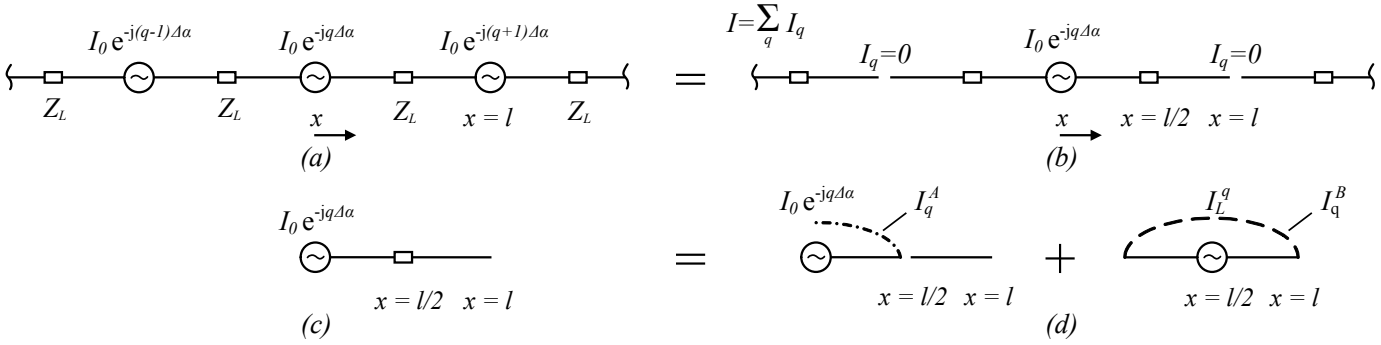

Fig. 7. Derivation of the current distribution: (a) whole row, (b) solution by superposition. (c) and (d) derivation of the current along the dipole by superposition of the generator q and the load equivalent generator.

To determine $I_q(x)$ in $0 \le x \le l$, we also substitute the load by an equivalent generator whose value is the current in the load when only the q generator is connected, I_L^q. Then, $I_q(x)$ in this region is given by the superposition of currents from the generator q, denoted as I_q^A, and the load equivalent generator, denoted as I_q^B, both fulfilling (27). Thus, $I_q(x) = I_q^A(x) + I_q^B(x)$ as schematically shown in Fig. 7(d). They are expressed as

$$I_q^A(x) = \begin{cases} \dfrac{I(0)\mathrm{e}^{-\mathrm{j}q\Delta\alpha}}{1-\mathrm{e}^{-\mathrm{j}\beta l}}\left(\mathrm{e}^{-\mathrm{j}\beta x} - \mathrm{e}^{\mathrm{j}\beta(x-l)}\right), & 0 \le x < l/2 \\ 0, & l/2 \le x \le l. \end{cases} \tag{28}$$

$$I_q^B(x) = \begin{cases} I_L^q \dfrac{\mathrm{e}^{-\mathrm{j}\beta x} - \mathrm{e}^{\mathrm{j}\beta x}}{\mathrm{e}^{-\mathrm{j}\beta l/2} - \mathrm{e}^{\mathrm{j}\beta l/2}}, & 0 \le x < l/2 \\ I_L^q \dfrac{\mathrm{e}^{\mathrm{j}\beta(x-l)} - \mathrm{e}^{-\mathrm{j}\beta(x-l)}}{\mathrm{e}^{-\mathrm{j}\beta l/2} - \mathrm{e}^{\mathrm{j}\beta l/2}}, & l/2 \le x \le l. \end{cases} \tag{29}$$

To determine I_L^q we use the telegrapher's equation for the current derivative:

$$\left(\left.\frac{\mathrm{d}I_q}{\mathrm{d}x}\right|_{l/2^-} - \left.\frac{\mathrm{d}I_q}{\mathrm{d}x}\right|_{l/2^+}\right) = \mathrm{j}\omega C I_L^q Z_L, \tag{30}$$

where $I_L^q Z_L = (V_{l/2^-} - V_{l/2+})$. Combining (28)-(30):

$$I_L^q = \frac{I(0)\mathrm{e}^{-\mathrm{j}q\Delta\alpha}}{(z_L+1)\mathrm{e}^{\mathrm{j}\beta l/2} - (z_L-1)\mathrm{e}^{-\mathrm{j}\beta l/2}}, \tag{31}$$

we have defined $z_L = Z_L/(2Z_c)$, and $\omega C = \beta/Z_c$ has been used. Z_c is the characteristic impedance of the wire. The current along the row due to generator q is then given by (28), (29) and (31), and it vanishes for $|x| \ge l$.

Let us solve now for the total current I, along the q element: the contributions to the right arm are given by I_q^A, I_q^B, and I_{q+1}^B. Similarly, for the left arm I_q^A, I_q^B, and I_{q-1}^B contribute. Note also the current due to the $q \pm 1$ generator takes the same form, only centered around $x' = x \mp l$. Hence, the current along the dipole q reads

$$I(x) = I(0)\mathrm{e}^{-\mathrm{j}q\Delta\alpha}\left[\frac{\mathrm{e}^{-\mathrm{j}\beta|x|} - \mathrm{e}^{\mathrm{j}\beta(|x|-l)}}{1-\mathrm{e}^{-\mathrm{j}\beta l}} + \frac{1+\Gamma_I}{2(\mathrm{e}^{\mathrm{j}\beta l/2} + \Gamma_I \mathrm{e}^{-\mathrm{j}\beta l/2})}\frac{\mathrm{e}^{-\mathrm{j}\beta|x|} - \mathrm{e}^{\mathrm{j}\beta|x|}}{\mathrm{e}^{-\mathrm{j}\beta l/2} - \mathrm{e}^{\mathrm{j}\beta l/2}}(1+\mathrm{e}^{\pm\mathrm{j}\Delta\alpha})\right]. \tag{32}$$

The minus sign in the exponential of (32) corresponds to the right arm and the plus sign to the left arm. Analogously to a transmission line, we have defined the current-wave reflection coefficient in the load as $\Gamma_I = (1-z_L)/(1+z_L)$. Note that, by superposition, $I(x)$ is also solution of (27). The current is quasi-periodic, forced by the excitation, and it is symmetric if $\Delta\alpha = 0$, as expected.

For an array composed of infinite rows, we will assume that the current along the row maintains the same shape. Coupling among the rows will be taken into account through Z_c, determined after. Under this assumption, it is clear that for H-plane scan the current along the row is the same as for broadside.

A. Special Cases

There are several important cases where $I(x)$ adopts a simple form. The first is broadside emission, where the current is symmetric. We can write ($q = 0$ element)

$$I(x) = I(0)\frac{\mathrm{e}^{\mathrm{j}\beta(l/2-|x|)} + \Gamma_I \mathrm{e}^{-\mathrm{j}\beta(l/2-|x|)}}{\mathrm{e}^{\mathrm{j}\beta l/2} + \Gamma_I \mathrm{e}^{-\mathrm{j}\beta l/2}}. \tag{33}$$

Then, at broadside (or H-plane scan), the asymptotic current distribution along the dipoles is that of a TL. In particular, for a disconnected array, assuming $\Gamma_I = -1$, it takes the familiar form $I(x) = I(0)\sin\beta(l/2 - |x|)/\sin(\beta l/2)$. For a connected array $\Gamma_I = 1$, and it takes the form $I(x) = I(0)\cos\beta(l/2 - |x|)/\cos(\beta l/2)$. In addition, for a disconnected array the current distribution is also independent of E-plane scan as it can be seen from (33). This is not the case for connected arrays, where the current takes the form:

$$I(x) = \frac{I(0)}{\mathrm{e}^{-\mathrm{j}\beta l} - \mathrm{e}^{\mathrm{j}\beta l}}\left[\mathrm{e}^{\mathrm{j}\beta|x|}(\mathrm{e}^{-\mathrm{j}\beta l} - \mathrm{e}^{\pm\mathrm{j}\Delta\alpha}) + \mathrm{e}^{-\mathrm{j}\beta|x|}(\mathrm{e}^{\pm\mathrm{j}\Delta\alpha} - \mathrm{e}^{\mathrm{j}\beta l})\right]. \tag{34}$$

The solid line in Fig. 8 shows the current distribution obtained from (34) for an array of connected dipoles scanning in the E-plane at 40°. The total phase change along the dipole equals $\Delta\alpha$, forced by the excitation, and can be easily noted in (33). For comparison, full-wave simulation results obtained for the same configuration by CST Studio Suite [31] are also plotted. As it can be seen, both curves are in good agreement. Near the dipole feed, where the current is minimum, the effect

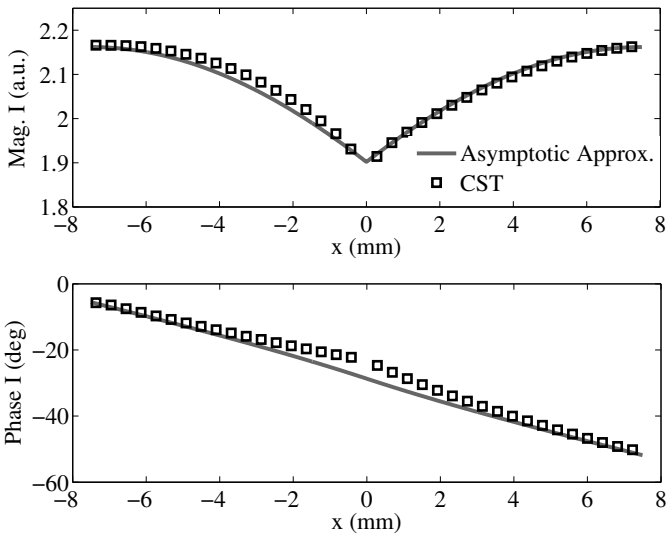

Fig. 8. Current distribution for an infinite phased array of connected dipoles in free-space scanning in E-plane at 40°. $p_x = p_y = l = \lambda/5$, and $w = \lambda/1000$.

of the radiation resistance causes some discrepancy in the phase as discussed in Section VIII. Finally, the results shown are also in agreement with the MoM analysis in [32].

B. The Asymptotic Equivalent Network at Broadside

In (33) we have seen that at broadside the current along the dipole is analogous to that of a TL. Therefore, X_0 can be retrieved from the network shown in Fig. 9(a). It is composed of a TL of length $l/2$ (as the dipole arm) terminated in Z_L. However, the characteristic impedance of the TL remains unknown.

Assuming TEM wave propagation, Z_c can be calculated from the inductance per unit length of the structure, L, using $Z_c = Lc/\sqrt{\epsilon_{\text{eff}}}$. The value of L is retrieved as follows: let a grid of vertical and parallel strips of width w and period p_y be illuminated by a plane wave at normal incidence, such that a uniform current distribution is excited along the strips, the electric field being parallel to the strips. The impedance of this structure has been studied in e. g. [27], [33], [34]. In particular, as discussed in [35], the inductance of the grid per strip and per unit length is given by

$$L = \frac{Z_0}{2\pi c} \ln\left(\frac{1}{\sin\left(\frac{\pi w}{2p_y}\right)}\right). \tag{35}$$

For the interface case, it is assumed that $\mu \approx \mu_0$ for both dielectrics, so L remains unaltered [27]. Finally, to account for the two arms of the dipole, the characteristic impedance of the network is given by $2Z_c$, twice that of the wire. This definition is also in agreement with the definition of z_L for Γ_I above.

Once the characteristic impedance of the TL is determined, it is worth mentioning that X_0 calculated with the equivalent network of Fig. 9(a) takes automatically into account the dipole end load, including disconnected dipoles ($Z_L \to \infty$).

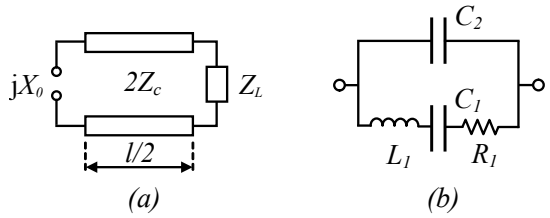

Fig. 9. (a) Equivalent network representing the scan reactance. (b) Equivalent lossy lumped element circuit that represents the scan impedance.

Now, it is possible to calculate the impedance for broadside emission (principal scan planes will be dealt with in Section VII). The current distribution for broadside given by (33) can be inserted in (9) to obtain the transformer relation, N, in the equivalent networks of Fig. 3 (interface) or Fig. 6 (interface and backing ground plane). Besides, X_0 can be obtained from the network of Fig. 9(a), where the inductance per unit length in (35) is used to calculate $2Z_c$.

Nevertheless, the asymptotic current approximation is only valid when w approaches 0 so that the scan impedance is mainly dominated by a reactance and the effect of the radiation resistance on the current distribution can be neglected. This approximation gives in general accurate results for thin dipoles except in the regions where the current at the dipole feed approaches zero (anti-resonance). In the latter case, (33) diverges at all times, independently of the dipole width, which is clearly wrong. To overcome this issue, and for more precise calculations, we have derived a lumped element circuit that accounts for variations in the stored energy and finite radiation losses in the impedance curves, as shown in Fig. 9(b). On the the other hand, we can rely on the simple networks to extract qualitative conclusions. For simplicity, we will restrict the analysis of the scan impedance when there is no ground plane in the cases of connected and disconnected dipoles.

To derive the lumped element circuit one can reason as follows: when losses are absent, it follows the curve of X_0 given by the network of Fig. 9(a). Then, L_1 and C_1 determine the resonance frequency as predicted by the TL ($X_0 = 0$), besides, L_1, C_1, and C_2 determine anti-resonance ($X_0 \to \pm\infty$). The third condition is to guarantee that the circuit yields the input reactance of the network model at low frequencies. Last, losses are included in the circuit by a lumped resistor R_1 so that the input resistance of the lumped element circuit is that of the network model when $f \to 0$. The values relating the different lumped elements with the network model are summarized in Table I for connected and disconnected dipoles. This circuit equivalent is valid up to, approximately, anti-resonance. An alternative circuit was developed in [36] but it utilizes the dipole auto-inductance. Furthermore, it is only valid for tightly coupled and connected arrays, and does not arise from a physical explanation of the scan impedance.

VI. Results for Broadside Emission

To test the validity of the proposed model, it is compared with full-wave simulations carried out with ANSYS HFSS [26]. For a central frequency of $f = 1$ cycle per unit-time that determines λ_c, the nominal parameters are: $p_x =$

TABLE I
LUMPED ELEMENT CIRCUIT PARAMETERS.

Parameter	Connected	Disconnected
L_1	Ll	$(C_1\omega_R^2)^{-1}$
C_1	∞	$3/16ln_{\text{eff}}^2/(Lc^2)$
C_2	$(L_1\omega_{AR}^2)^{-1}$	$C_1/3$
R_1	$R_{r,f\to 0}$	$16/9R_{r,f\to 0}$
ω_{AR}	$\pi c/(n_{\text{eff}}l)$	$2\pi c/(n_{\text{eff}}l)$
ω_R	0	$\pi c/(n_{\text{eff}}l)$

$p_y = \lambda_{c,\text{eff}}/2$, $l = 1.0p_x$ (connected) or $0.9p_x$ (disconnected), $w = \lambda_{c,\text{eff}}/1000$, and feed port length $\lambda_{c,\text{eff}}/100$. The array is freestanding or in a vacuum-dielectric interface. In the following, results are presented for a variation of one nominal parameter at a time. The calculated values in Figs. 10-11 have been obtained using the lumped element circuit in Fig. 9(b) explained in the preceding section.

A. Varying End Load

The resonant behavior of dipole arrays is highly dependent on the load and can be simply examined by inspection of the input reactance in the equivalent network of Fig. 9(a). For connected dipoles $X_0 = 2Z_c\tan(\beta l/2)$, therefore resonances occur at $l/\lambda = n$ with n a natural number, whereas anti-resonances occur at $l/\lambda = n + 1/2$. In the latter, the open circuit condition is effectively achieved and $I(0) = 0$, consequently, R_r will diverge too. Conversely, for disconnected arrays of dipoles, $X_0 = -2Z_c/\tan(\beta l/2)$ and the resonant/anti-resonant frequencies will be swapped with respect to connected dipoles of the same length (see for instance Fig. 11). This fundamental difference between connected and disconnected dipoles stems from the fact that in the former the maximum current occurs at the dipole end ($\Gamma_I = 1$) whereas, for disconnected dipoles, the current at the edge is always minimum ($\Gamma_I = -1$). The π phase difference in the reflection coefficient is responsible for the $\lambda/2$ shift of the resonances. In the usual case of capacitively loaded dipoles, the phase of the reflection coefficient for the current-wave lies between the previous cases, then the resonances lie between the aforementioned limiting cases. Furthermore, the fact that connected dipoles show resonant response at low frequencies makes them amenable to array design with large scan angles. In this case, the lattice can be kept $< \lambda/2$, whereas for disconnected dipoles $p_x > \lambda/2$ limited by the resonant length of the dipole. This is even more evident for a dielectric interface, where the required spacing to avoid grating lobes is $\lambda/(2n_2)$ but the dipole length scales down only as n_{eff}.

B. Varying ϵ_r

Practical array designs require printing the antennas on an interface, for mechanical support or to diminish the effect of a ground plane. In the latter case, it is more convenient to position the ground plane in the medium with lower dielectric index for a broadband design, since it renders the impedance less dependent on frequency. Also, it is to be observed that the short-circuit will occur at DC and certain frequencies regardless of the interface, hence, imposing a fundamental limit in the absolute impedance bandwidth of the array.

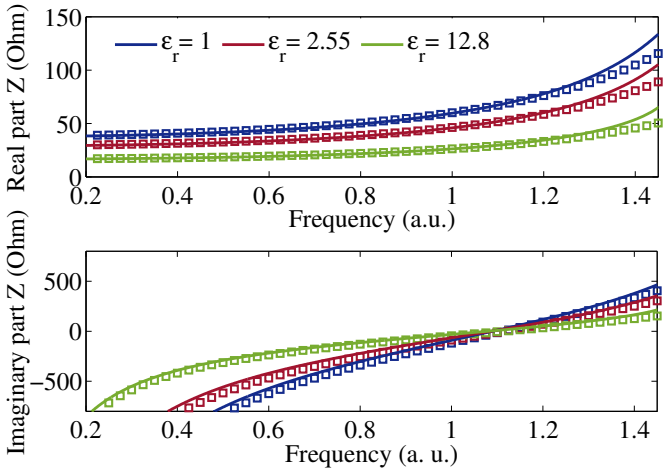

Fig. 10. Real and imaginary parts of the broadside impedance for disconnected dipoles: simulated (solid lines), and calculated (squares) for three different relative permittivities of the substrate.

As shown in the previous subsection, X_0 is proportional to Z_c and in turn to $1/\sqrt{\epsilon_{\text{eff}}}$ for connected or disconnected dipoles. Thus, a high permittivity dielectric substrate flattens the dipole reactance. Fig. 10 shows the variation of the simulated and calculated broadside impedance with ϵ_r for disconnected dipoles. ϵ_r corresponds to the relative permittivity of the substrate when the array is printed in an air-dielectric interface as shown in Fig. 1(b). It is important to note that p_x, and p_y are scaled by $\lambda_{c,\text{eff}}$ and so the dipole electrical length remains fixed as seen in Fig. 10.

C. Varying Dipole Width

Fig. 11 shows the simulated and calculated broadside impedance for different dipole widths for connected (a), and disconnected (b) dipoles. If we calculated the scan resistance from the asymptotic current approximation in (33), where Γ_I does not depend on w, it would yield a result also independent on w. In practice, this is true only for regions far away from anti-resonance. As w increases, the resonance quality factor decreases, and the impedance curves are affected. The lossy lumped element circuit predicts this behavior reasonably well for connected dipoles, as shown in Fig. 11(a). However, for disconnected dipoles the model loses validity. In particular, variations of effective dipole length with dipole width are not taken into account. We will discuss it in more detail in Section VIII. Finally, note a wider dipole yields a flatter reactance, as can be inferred from (35).

D. Varying Lattice (p_x, p_y)

The dipole length has been defined as 100% or 90% of p_x, therefore, variations in p_x would scale the curves accordingly. Conversely, variations in p_y influence the coupling among neighboring rows, and can be used to modify the impedance.

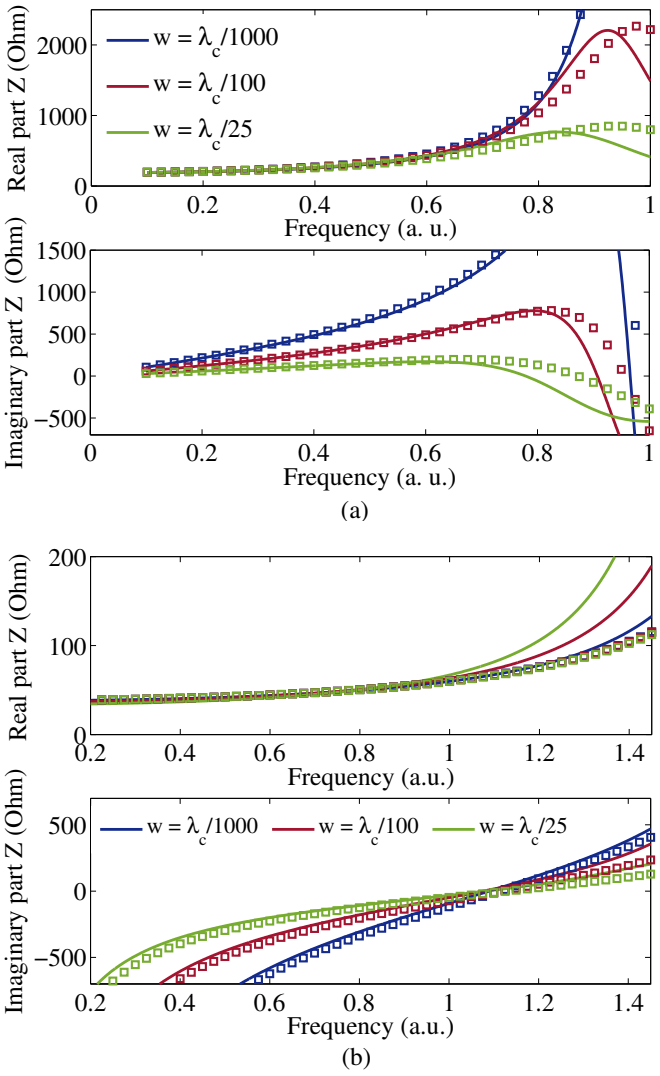

Fig. 11. Real and imaginary parts of the broadside impedance: simulated (solid lines), and calculated (squares) for three different dipole widths. (a) connected dipoles, (b) disconnected dipoles.

From the network model we can observe that the factor N^2 is inversely proportional to p_y. Since within this approximation the current distribution does not change with p_y for connected or disconnected dipoles, R_r scales inversely proportional to p_y. On the other hand, from (35), L decreases with p_y, so narrower spacing decreases X_0 and flattens the dipole reactance. Coupling, as is clear from the network model, can be used to obtain broadband arrays.

VII. Extension for Principal Scan Planes

In section V, we have seen that at broadside emission the current distribution along the dipole in asymptotic approximation is that of a transmission line. Therefore, it was possible to identify X_0 with the equivalent network of Fig. 9(a), and ultimately compute the scan impedance at broadside using a lossy lumped element circuit. For scan in the principal planes, we need to examine the variations of the inductance per unit length on the equivalent TL and of the current distribution, if any.

The inductance of a grid of strips for a plane wave in oblique incidence with the tangent electric field parallel to the wires was calculated in [34, Ch. 4]. We can express the grid inductance per unit length as

$$L = \frac{Z_0}{2\pi c} \ln\left(\frac{1}{\sin\left(\frac{\pi w}{2p_y}\right)}\right)\left(1-\cos^2\phi\sin^2\theta\right). \qquad (36)$$

For H-plane scan, $\phi = 90°$, and L does not change. Also, according to our model, the current is the same as for broadside. Therefore, it is still possible to compute the impedance with the lossy lumped element circuit and extract conclusions from the network model. Results calculated using the lossy lumped element circuit for an array of connected dipoles are shown in Fig. 12(a) for different scan angles and nominal array parameters. As radiation losses increase while L is maintained, anti-resonance becomes wider and flatter, and this behavior is well captured. Conversely, the equivalent network would predict that X_0 is maintained and R_r is scaled by $1/\cos\theta$ because it does not capture the consequences of a lower quality factor in the resonance. This is specially clear at large scan angles. Finally, for scan at $80°$ near $f = 1$ a.u. the curve deviates from simulation as the onset of a grating lobe is approached.

For E-plane scan, we need to distinguish between connected and disconnected dipoles. In the latter case, the current in (32) is the same as for broadside emission, so X_0 remains the same and R_r scales with $\cos\theta$. Note that, even if in (36) L varies, this is for a plane wave in oblique incidence that generates a linear phase progression along the wires of the grid. For the array of disconnected dipoles, there is no linear phase progression, and the expression for L at broadside has to be used.

On the other hand, for connected dipoles, the scan impedance can be obtained as follows: the current at the dipole feed is $I(0)$, whereas the voltage is the superposition of the voltages impressed by all generators in $x = 0$. As we have seen before, for the q element, only $q-1$, q, $q+1$ contribute to the current. When only the q generator is active, we use the fact that the current along the dipole is that of an open-ended transmission line of length l. The dipole self-reactance is then $Z_{q,q} = V^q(0)/I(0) = -\mathrm{j}2Z_c/\tan(\beta l)$. When only one of the $q \pm 1$ generators is on, the voltage at the dipole feed corresponds to that of the open-ended transmission line of length l at the position of the load, so $Z_{q\pm1,q} = V^{q\pm1}(x=0)/I(0) = \mathrm{j}Z_c\mathrm{e}^{\pm\Delta\alpha}/\sin(\beta l)$. Thus, the scan reactance is given by the sum of the three terms:

$$X_0 = 2Z_c\left(\frac{\cos\Delta\alpha}{\sin(\beta l)} - \frac{1}{\tan(\beta l)}\right). \qquad (37)$$

It is interesting to note that (37) reduces to $2Z_c\tan(\beta l/2)$ when $\Delta\alpha = 0$ and is an alternative way to calculate the scan reactance based on mutual impedances. Fig. 12(b) shows the results for an array of connected dipoles and nominal array configuration. Calculations are performed inserting the current distribution given by (34) in (9) to calculate R_r from the network of Fig. 3. X_0 is calculated using (37). In this case, the current distribution no longer follows that of a TL, and it is not

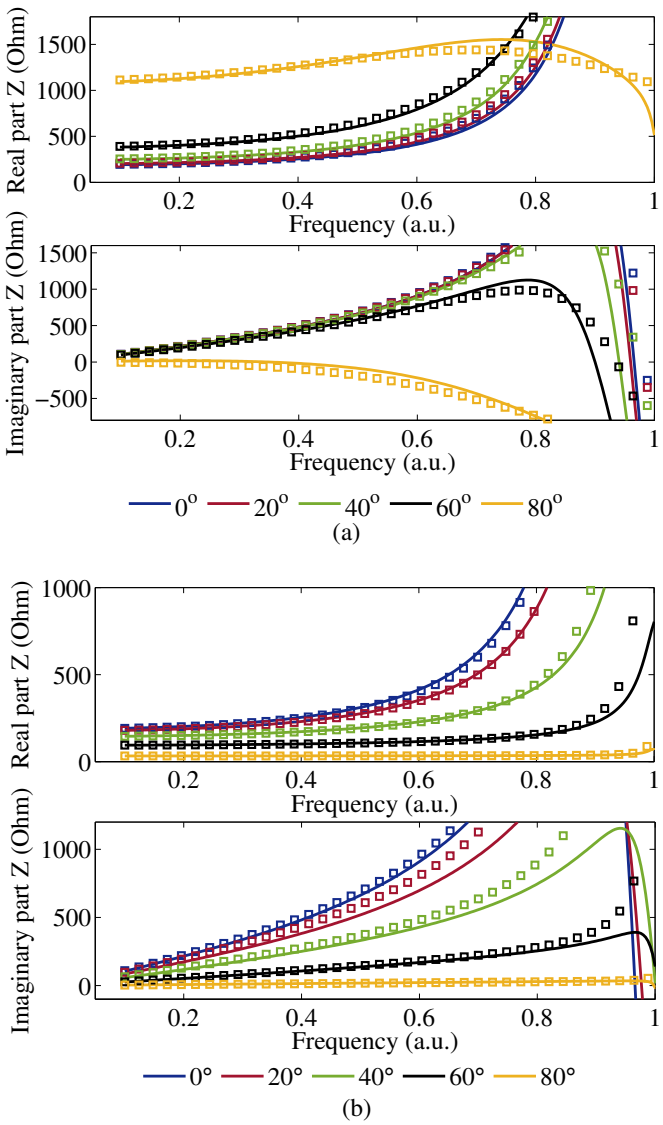

Fig. 12. Real and imaginary parts of the scan impedance: simulated (solid lines), and calculated (squares) for a connected array of dipoles at different scan angles in (a) H-plane, and (b) E-plane.

possible to map the impedance curves with the lossy lumped element circuit used before, causing the model to deviate close to anti-resonance.

VIII. Limitations of the Model

As already mentioned, the asymptotic current approximation neglects the effect on the current due to the radiation resistance. It constitutes a term in quadrature with the current impressed by the generator and the distribution is that of a reflecting antenna, as noted by [30]. Since $Rr \neq 0$, this term is present event when $w \to 0$ and it dominates the current at the dipole input terminals at anti-resonance when the asymptotic current distribution approaches zero and the impedance takes a maximum value. Thus, in this region, the TL model loses validity. This limitation can be overcome for the interfacial array by using a lossy lumped element except for E-plane scan with connected dipoles. In general, multilayered media or a ground plane will affect R_r and so, the associated term in the current distribution. On the other hand, following the discussion of [30], the asymptotic current distribution stems from a TEM wave that propagates along a linear antenna. When discontinuities exist, such as at the ends of disconnected dipoles, a TEM wave cannot match the boundary conditions and higher-order waves must exist. They will have an impact on the current distribution. In particular, it results in the model being more accurate for connected dipoles than for disconnected ones. Similarly, it is known that as a grating lobe is close to its onset, it affects the scan impedance [1, Ch. 7], then, in this case, some deviation from the model should be expected. Last, the expression for L becomes invalid if the spacing is comparable to the wavelength [27]. In this case, it is invalid when grating lobes appear and the inductance of the grid can no longer be expressed by a single lumped element.

Finally, as for the inclusion of a ground plane, a comparative of the network model (Figs. 3 and 6) with full-wave simulations shows $Z_d = 55.7 - \mathrm{j}109.4\ \Omega$ versus $Z_d = 59.7 - \mathrm{j}91.0\ \Omega$ respectively, when there is no ground plane, and $Z_d = 111.4 - \mathrm{j}109.4\ \Omega$ versus $Z_d = 118.6 - \mathrm{j}98.6\ \Omega$ respectively, for a ground plane at $d = \lambda/4$. The numbers correspond to an array of nominal parameters (as detailed in Section VI) for $f = 1$ and disconnected dipoles, and indicate that the model is still valid.

IX. Conclusion

A model has been presented to determine the scan impedance of infinite phased arrays of dipoles at a dielectric interface. First, equivalent circuits and expressions for the scan resistance in the principal scan planes are derived using the boundary conditions for the fundamental Floquet mode. This derivation provides a straightforward interpretation of the role played on the scan impedance by the pattern of the Hertzian dipole, apparent allocated area, or partially stationary waves formed by the presence of a ground plane or interface. Using such boundary conditions, closed-form expressions have also been derived for the ratio of intensity radiated towards each half-space of the interfacial array. Second, an asymptotic approximation is introduced to determine the current along the array. Besides, the scan reactance is related to the inductance per unit length of an inductive grid of strips. To perform the calculations of the scan impedance, a lossy lumped element circuit is generally preferred because it conveniently removes the divergence of the impedance at anti-resonance of the asymptotic approximation, and it also accounts for variations in the impedance curves associated with the quality factor of the resonance. The model shows how fundamental differences in the current distribution between connected and disconnected dipoles relate to different impedance curves at broadside and in the principal scan planes. Indeed, the derivation of a model based on physical grounds has permitted us to illustrate with equivalent circuits and simple expressions how the principal array variables affect the scan impedance.

References

[1] R. C. Hansen, *Phased Array Antennas*, 2nd ed. Wiley, 2009.

[2] A. K. Bhattacharyya, *Phased Array Antennas: Floquet Analysis, Synthesis, BFNs and Active Array Systems*. Wiley-Interscience, 2006.

[3] C. Craeye and D. González-Ovejero, "A review on array mutual coupling analysis," *Radio Sci.*, vol. 46, no. 02, pp. 1–25, 2011.

[4] M. Jones and J. Rawnick, "A new approach to broadband array design using tightly coupled elements," in *MILCOM 2007 - IEEE Mil. Commun. Conf.*, Oct 2007, pp. 1–7.

[5] S. S. Holland and M. N. Vouvakis, "The planar ultrawideband modular antenna (PUMA) array," *IEEE Trans. Antennas Propag.*, vol. 60, no. 1, pp. 130–140, Jan 2012.

[6] D. Cavallo and A. Neto, "A connected array of slots supporting broadband leaky waves," *IEEE Trans. Antennas Propag.*, vol. 61, no. 4, pp. 1986–1994, Apr 2013.

[7] D. Pozar, "Analysis of finite phased arrays of printed dipoles," *IEEE Trans. Antennas Propag.*, vol. 33, no. 10, pp. 1045–1053, Oct 1985.

[8] H. Wheeler, "Simple relations derived fom a phased-array antenna made of an infinite current sheet," *IEEE Trans. Antennas Propag.*, vol. 13, no. 4, pp. 506–514, July 1965.

[9] D. Pozar, "General relations for a phased array of printed antennas derived from infinite current sheets," *IEEE Trans. Antennas Propag.*, vol. 33, no. 5, pp. 498–504, May 1985.

[10] L. Stark, "Radiation impedance of a dipole in an infinite planar phased array," *Radio Sci.*, vol. 1, no. 3, pp. 361–377, Mar 1966.

[11] B. L. Diamond, "A generalized approach to the analysis of infinite planar array antennas," *Proc. IEEE*, vol. 56, no. 11, pp. 1837–1851, Nov 1968.

[12] R. C. Hansen, *Microwave Scanning Antennas, Vol. II: Array Theory and Practice*. New York: Academic, 1966.

[13] V. W. H. Chang, "Infinite phased dipole array," *Proc. IEEE*, vol. 56, no. 11, pp. 1892–1900, Nov 1968.

[14] M. Kominami, D. Pozar, and D. Schaubert, "Dipole and slot elements and arrays on semi-infinite substrates," *IEEE Trans. Antennas Propag.*, vol. 33, no. 6, pp. 600–607, June 1985.

[15] R. C. Hansen, "Non-Foster and connected planar arrays," *Radio Sci.*, vol. 39, no. 4, pp. 1–14, Aug 2004.

[16] C. Mias and A. Freni, "Application of Wait's formulation to connected array antennas," *IEEE Antennas Wireless Propag. Lett.*, vol. 12, pp. 1535–1538, 2013.

[17] A. Neto, D. Cavallo, G. Gerini, and G. Toso, "Scanning performances of wideband connected arrays in the presence of a backing reflector," *IEEE Trans. Antennas Propag.*, vol. 57, no. 10, pp. 3092–3102, Oct 2009.

[18] D. Cavallo, A. Neto, and G. Gerini, "Green's function based equivalent circuits for connected arrays in transmission and in reception," *IEEE Trans. Antennas Propag.*, vol. 59, no. 5, pp. 1535–1545, May 2011.

[19] D. Cavallo, A. Neto, and G. Gerini, "Analytical description and design of printed dipole arrays for wideband wide-scan applications," *IEEE Trans. Antennas Propag.*, vol. 60, no. 12, pp. 6027–6031, Dec 2012.

[20] E. A. Alwan, K. Sertel, and J. L. Volakis, "Circuit model based optimization of ultra-wideband arrays," in *Proc. 2012 IEEE Int. Symp. Antennas Propag.*, July 2012, pp. 1–2.

[21] Y. Zhou *et al.*, "Tightly coupled array antennas for ultra-wideband wireless systems," *IEEE Access*, vol. 6, pp. 61 851–61 866, 2018.

[22] B. A. Munk, *Frequency Selective Surfaces: Theory and Design*. Wiley-Blackwell, 2000.

[23] ——, *Finite Antenna Arrays and FSS*. Wiley-Interscience, 2003.

[24] S. N. Makarov, A. Puzella, and V. Iyer, "Scan impedance for an infinite dipole array: Accurate theoretical model compared to numerical software," *IEEE Antennas Propag. Mag.*, vol. 50, no. 6, pp. 132–149, 2008.

[25] N. Engheta, C. H. Papas, and C. Elachi, "Radiation patterns of interfacial dipole antennas," *Radio Sci.*, vol. 17, no. 06, pp. 1557–1566, Nov 1982.

[26] ANSYS, "High Frequency Structure Simulator," 2019, ver. 19.0.0.

[27] O. Luukkonen *et al.*, "Simple and accurate analytical model of planar grids and high-impedance surfaces comprising metal strips or patches," *IEEE Trans. Antennas Propag.*, vol. 56, no. 6, pp. 1624–1632, June 2008.

[28] D. Pozar and D. Schaubert, "Scan blindness in infinite phased arrays of printed dipoles," *IEEE Trans. Antennas Propag.*, vol. 32, no. 6, pp. 602–610, June 1984.

[29] G. D. Alley, "Interdigital capacitors and their application to lumped-element microwave integrated circuits," *IEEE Trans. Microw. Theory Techn.*, vol. 18, no. 12, pp. 1028–1033, 1970.

[30] S. A. Schelkunoff and H. T. Friis, "Antenna current," in *Antennas: Theory and Practice*. Wiley, 1952.

[31] Computer Simulation Technology, "CST Studio Suite," ver. 2018.

[32] R. Hansen, "Linear connected arrays [coupled dipole arrays]," *IEEE Antennas Wireless Propag. Lett.*, vol. 3, pp. 154–156, 2004.

[33] L. B. Whitbourn and R. C. Compton, "Equivalent-circuit formulas for metal grid reflectors at a dielectric boundary," *Appl. Opt.*, vol. 24, no. 2, pp. 217–220, Jan 1985.

[34] S. Tretyakov, "Periodical structures, arrays and meshes," in *Analytical Modelling in Applied Electromagnetics*. Artech House, 2003.

[35] G. G. Macfarlane, "Quasi-stationary field theory and its application to diaphragms and junctions in transmission lines and wave guides," *J. IEE - Part IIIA: Radiolocation*, vol. 93, no. 4, pp. 703–719, 1946.

[36] B. Riviere, H. Jeuland, and S. Bolioli, "New equivalent circuit model for a broadband optimization of dipole arrays," *IEEE Antennas Wireless Propag. Lett.*, vol. 13, pp. 1300–1304, 2014.

Álvaro J. Pascual received the B.Sc. degree in Physics from the University of Zaragoza in 2015, and the M.Sc. degree in Photonics (cum laude) from the Polytechnic University of Catalonia (UPC) in 2016. During 2015-2016 he was a research assistant at the Group of Optical Communications at UPC. He was an R&D intern with Aragon Photonics Labs (Zaragoza) in the summer of 2015, and with Melexis Technologies NV (Tessenderlo, Belgium) in the last third of 2016. Since November 2017 he works towards the PhD degree in Electronic Engineering at the Institute of Electronics and numeRical Technologies (IETR) in Rennes, France. In 2019 was a visiting student at the Group of Photonic Technologies and the Radiofrequency and Antennas Group at University Carlos III, Madrid, Spain. His research interests include photonic-enabled mm-wave antenna arrays and phased array antenna theory. Among other journals, Mr. Pascual has served as a reviewer of IEEE Transactions on Antennas and Propagation.

Ronan Sauleau (M'04–SM'06–F'18) graduated in electrical engineering and radio communications from the Institut National des Sciences Appliquées, Rennes, France, in 1995. He received the Agrégation degree from the Ecole Normale Supérieure de Cachan, France, in 1996, and the Doctoral degree in signal processing and telecommunications and the "Habilitation à Diriger des Recherches" degree, both from the University of Rennes 1, France, in 1999 and 2005, respectively.

He was an Assistant Professor and Associate Professor at the University of Rennes 1, between September 2000 and November 2005, and between December 2005 and October 2009, respectively. He has been appointed as a full Professor in the same University since November 2009. His current research fields are numerical modeling (mainly FDTD), millimeter-wave printed and reconfigurable (MEMS) antennas, substrate integrated waveguide antennas, lens-based focusing devices, periodic and non-periodic structures (electromagnetic bandgap materials, metamaterials, reflectarrays, and transmitarrays) and biological effects of millimeter waves. He has been involved in more than 60 research projects at the national and European levels and has co-supervised 23 post-doctoral fellows, 44 PhD students and 50 master students.

He has received 17 patents and is the author or coauthor of more than 260 journal papers and 510 publications in international conferences and workshops. He has shared the responsibility of the research activities on antennas at IETR in 2010 and 2011. He was co-director of the research Department 'Antenna and Microwave Devices' at IETR and deputy director of IETR between 2012 and 2016. He is now director of IETR. Prof. Sauleau received the 2004 ISAP Conference Young Researcher Scientist Fellowship (Japan) and the first Young Researcher Prize in Brittany, France, in 2001 for his research work on gain-enhanced Fabry-Perot antennas. In September 2007, he was elevated to Junior member of the "Institut Universitaire de France". He was awarded the Bronze medal by CNRS in 2008, and the silver medal in 2020. He was the co-recipient of several international conference awards with some of his students (Int. Sch. of BioEM 2005, BEMS'2006, MRRS'2008, E-MRS'2011, BEMS'2011, IMS'2012, Antem'2012, BioEM'2015, EuCAP'2019). He served as a guest editor for the IEEE Antennas Propogat. Special Issue on "Antennas and Propagation at mm and sub mm waves". He served as a national delegate for several EU COST actions. He has served as a national delegate for EurAAP and as a member of the board of Director of EurAAP from 2013 to 2018.

David González-Ovejero (S'01–M'13–SM'17) was born in Gandía, Spain, in 1982. He received the telecommunication engineering degree from the Universidad Politécnica de Valencia, Valencia, Spain, in 2005, and the Ph.D. degree in electrical engineering from the Université catholique de Louvain, Louvain-la-Neuve, Belgium, in 2012.

From 2006 to 2007, he was as a Research Assistant with the Universidad Politécnica de Valencia. In 2007, he joined the Université catholique de Louvain, where he was a Research Assistant until 2012. From 2012 to 2014, he worked as Research Associate at the University of Siena, Siena, Italy. In 2014, he joined the Jet Propulsion Laboratory, California Institute of Technology, Pasadena, CA, USA, where he was a Marie Curie Postdoctoral Fellow until 2016. Since then, he has been a Research Scientist with the French National Center for Scientific Research (CNRS), appointed at the Institut d'Electronique et de Télécommunications de Rennes, France.

Dr. González-Ovejero was a recipient of a Marie Curie International Outgoing Fellowship from the European Commission in 2013, the Sergei A. Schelkunoff Transactions Prize Paper Award from the IEEE Antennas and Propagation Society in 2016, and the Best Paper Award in Antenna Design and Applications at the 11th European Conference on Antennas and Propagation in 2017. Since 2019, he has been an Associate Editor of the IEEE Transactions on Antennas and Propagation and the IEEE Transactions on Terahertz Science and Technology.